J Physiol 588.18 (2010) pp 3499–3509

The Journal of Physiology

Hormonal inhibition of endocytosis: novel roles for noradrenaline and G protein G_z

Ying Zhao[1,2], Qinghua Fang[2], Susanne G. Straub[1], Manfred Lindau[2] and Geoffrey W. G. Sharp[1]

[1] *Department of Molecular Medicine, Cornell University, Ithaca, NY 14853, USA*
[2] *School of Applied and Engineering Physics, Cornell University, Ithaca, NY 14853, USA*

The modulation of endocytosis following exocytosis by noradrenaline (NA), a physiological inhibitor of insulin secretion, was investigated in INS 832/13 cells using patch-clamp capacitance measurements. Endocytosis was inhibited by NA in a pertussis toxin-insensitive manner. Dialysing a synthetic peptide mimicking the C-terminus of the α-subunit of G_z into the cells blocked the inhibition of endocytosis by NA. Cell-attached capacitance measurements indicated that inhibition by NA was due to a decreased number of endocytotic events without a change in vesicle size. Analysis of fission pore closure kinetics revealed two distinct fission modes, with NA selectively inhibiting the rapid fission pore closure events. Comparison of the actions of NA and deltamethrin, a calcineurin antagonist and potent inhibitor of endocytosis, demonstrated that they inhibit endocytosis by different mechanisms. These findings establish novel actions for NA and G_z in insulin-secreting cells and possibly other cell types.

(Received 16 March 2010; accepted after revision 14 July 2010; first published online 19 July 2010)
Corresponding author G. W. G. Sharp: Department of Molecular Medicine, Cornell University, Ithaca, NY 14853-6401, USA. Email: gws2@cornell.edu

Abbreviations C_v, vesicle capacitance; DM, deltamethrin; G_p, fission pore conductance; Im, imaginary part of the patch admittance; NA, noradrenaline; PTX, pertussis toxin; Re, real part of the patch admittance; RRP, readily releasable pool.

Introduction

Noradrenaline (NA), a well-known inhibitor of insulin secretion, acts via multiple pathways to inhibit secretion (Sharp, 1996). These include activation of K^+ channels to repolarize or hyperpolarize the cell (Rorsman *et al.* 1991; Schermerhorn & Sharp, 2000; Sieg *et al.* 2004) and thus reverse or prevent depolarization and the consequent opening of voltage-dependent Ca^{2+} channels. Adenylyl cyclase is inhibited (Komatsu *et al.* 1995), thus preventing the augmentation of stimulated insulin release via incretins such as glucagon-like peptide 1. Importantly, a 'distal' effect that occurs downstream of increased $[Ca^{2+}]_i$ blocks exocytosis *per se* (Sharp *et al.* 1989; Ullrich & Wollheim, 1989; Sharp, 1996). The latter effect, inhibition of exocytosis at the distal site, has its parallel in the CNS where inhibition of neurotransmitter release (e.g. by serotonin) is also exerted by an effect on exocytosis downstream of increased $[Ca^{2+}]_i$ (Blackmer *et al.* 2001).

Until recently, it was thought that all of these inhibitory effects in the β-cell were mediated by the pertussis toxin (PTX)-sensitive heterotrimeric G_i and G_o proteins (Komatsu *et al.* 1995). However, it has been reported that inhibition of adenylyl cyclase by PGE_1 is mediated via G_z (Kimple *et al.* 2005, 2008) thus opening up the possibility of other G_z-mediated events in the β-cell.

Release of neurotransmitters and hormones by exocytosis is rapidly followed by compensatory endocytosis, which recaptures the added membrane and thereby maintains cellular homeostasis (Jahn *et al.* 2003). Endocytotic pathways are generally classified as either 'conventional', which involves recruitment of clathrin and a group of adaptor proteins, and/or 'rapid', e.g. by 'kiss and run' (Ales *et al.* 1999; Harata *et al.* 2006; Rizzoli & Jahn, 2007). The Ca^{2+}-dependence of endocytosis has been best characterized in synaptic systems and neuroendocrine cells (Ales *et al.* 1999; Jarousse & Kelly, 2001; Artalejo *et al.* 2002; Murthy & De Camilli, 2003). Despite the achievements in understanding the dynamics of vesicle recycling and the role of Ca^{2+} in membrane retrieval, nothing is known about the hormonal regulation of endocytosis. Here we show that NA inhibits endocytosis. Whole-cell capacitance measurements (Lindau & Neher, 1988) were performed to detect changes in the entire plasma membrane area, and cell-attached capacitance measurements (Debus & Lindau, 2000; Dernick *et al.* 2003) to examine endocytosis at the single vesicle level.

DOI: 10.1113/jphysiol.2010.190116

Methods

Cell culture

INS 832/13 cells (a kind gift from Dr C. B. Newgard) were cultured in complete RPMI-1640 medium supplemented with 10% fetal bovine serum, 100 μg ml^{-1} streptomycin and 100 U ml^{-1} penicillin at 37°C in a 95% air–5% CO_2 atmosphere.

Standard whole-cell patch-clamp and capacitance measurements

Patch electrodes were made from borosilicate glass capillaries. The pipette resistances ranged from 2 to 3 MΩ when filled with the intracellular solutions. Data were acquired using a PULSE 8.75-controlled EPC-10 amplifier (HEKA). The change in cell capacitance was estimated by the Lindau–Neher technique as implemented by the 'Sine+DC' feature of the lock-in software module (500 Hz, 40 mV peak-to-peak amplitude, −70 mV DC-holding potential). The current signals were digitized at 10 kHz. The data were analysed with the customized IgorPro routines (WaveMetrics, Inc.). The standard extracellular solution contained (in mM): 120 NaCl, 20 TEA-Cl, 2.6 $CaCl_2$, 5.6 KCl, 1.2 $MgCl_2$, 10 glucose and 10 Hepes-NaOH (pH 7.4). The pipette solution contained (in mM): 145 caesium glutamate, 8 NaCl, 0.18 $CaCl_2$, 0.28 BAPTA, 1 $MgCl_2$, 2 ATP-Mg, 0.5 GTP-Na_2, 0.3 cAMP, 10 Hepes-CsOH (pH 7.3), and 300 nM calculated free $[Ca^{2+}]_i$. Na^+ currents were blocked by 500 nM TTX. All the chemicals were freshly prepared before the experiments. The final extracellular concentration of NA was 10 μM. The final intracellular concentration of deltamethrin was 1 μM. The synthesized peptides and PTX were purchased from GenScript and Sigma Co., respectively. The whole-cell membrane capacitance (C_m) recordings were performed at 32–35°C.

Cell-attached capacitance measurements

After wax-coating and fire-polishing, the pipette tips had a resistance of >1 MΩ when filled with pipette solution containing (in mM): 50 NaCl, 100 TEA-Cl, 5 KCl, 1 $MgCl_2$, 5 $CaCl_2$, 10 Hepes-NaOH (pH 7.3). The cells were plated on 8 mm coverslips and continuously bathed in a ∼70 μl solution containing (in mM): 130 NaCl, 5 KCl, 1 $MgCl_2$, 5 $CaCl_2$, 10 glucose, and 10 Hepes-NaOH (pH 7.3). The final concentrations of NA and deltamethrin in the bath solution were 10 μM for each. For capacitance measurements, the holding potential of 0 mV was added to the sine wave (50 mV r.m.s., 20 kHz) from the lock-in amplifier (SR830 DSP Stanford Research Systems) and fed into the stimulus input of the patch-clamp amplifier. The C-slow compensation of the EPC-7 (HEKA) was set to 0.2 pF, the G-series compensation to 0.2 pS. The pipette current was filtered by the built-in 10 kHz filter of the patch-clamp amplifier and scaled down by a factor of 10 before input to the lock-in amplifier. The correct phase for the lock-in amplifier was found by utilizing a capacitance dither switch on the patch-clamp amplifier. At the correct phase, the lock-in amplifier computed the real (Re) and the imaginary (Im) part of the pipette current, which was recorded by the 16-bit ADC as Y1 and Y2, respectively. The output filter of the lock-in amplifier was set to 1 ms time constant, 24 dB octave^{-1}. After the recording, the calibration pulses were used to convert units of the Y1 and Y2 traces from raw counts into pS and fF, respectively. Capacitance steps were reliably detected for step sizes >0.1 fF. Smaller steps were not included in the analysis. Typically the fission pore closing manifests itself as a transient decrease in the Re of the patch admittance associated with or without a time-resolved increase in the Im. The cell-attached C_m recordings were performed at room temperature.

Data analysis

All values are presented as mean ± S.E.M. Significance was determined either by Student's *t* test or by ANOVA followed by Fisher's least significant difference test as appropriate.

Results

Inhibition of endocytosis by NA

When control or NA-treated cells were stimulated by a short train of 500 ms pulses (5 pulses, from −70 mV to +10 mV, 300 ms interpulse interval), the capacitance increases evoked by the 1st pulses were robust in both groups of cells. This is because the high Ca^{2+} influx associated with these conditions blocks the inhibitory effect of NA on exocytosis (Zhao *et al.* 2010, accompanying paper). However, the capacitance increases responding to the subsequent pulses had much smaller amplitude. This is due to the depletion of the readily releasable pool of granules (RRP) by the 1st pulse and an interpulse interval of 300 ms that was insufficient for the RRP to be refilled. Following the stimulation of exocytosis, endocytosis is indicated by a decrease of cell membrane capacitance (negative ΔC_m). The endocytosis observed during the four interpulse intervals and the 300 ms interval following the last pulse was termed early endocytosis ($\Delta C_m/_{\text{early-endo}}$, shown with high time resolution in Fig. 1*A* right) and was quantified as the sum of the endocytosis occurring during the 300 ms intervals following the five individual pulses. After the pulse train, the subsequent endocytosis was continuously monitored for ∼75 s while the cell membrane potentials

were clamped at −70 mV (Fig. 1*A* left). This was termed late endocytosis ($\Delta C_m/_{late\text{-}endo}$). The late endocytosis was determined as the maximal decrease of cell capacitance within the 75 s period starting 300 ms after the last stimulus pulse. Of interest is the fact that the negative ΔC_m due to endocytosis greatly exceeded the positive ΔC_m of the preceding exocytosis (see control trace in Fig. 1*A*). Quantitative analysis revealed significant hormonal inhibition of both phases of endocytosis by NA (Fig. 1*B*, $\Delta C_m/_{early\text{-}endo}$: control, -27.5 ± 3.2 fF pF^{-1}, $n = 34$ cells; NA, -12.2 ± 1.6 fF pF^{-1}, $n = 28$ cells, $P < 0.01$. $\Delta C_m/_{late\text{-}endo}$: control, -55.2 ± 5.3 fF pF^{-1}, $n = 34$ cells; NA, -35.8 ± 3.3 fF pF^{-1}, $n = 28$ cells, $P < 0.05$). While both kinetic phases were reduced in amplitude, NA inhibition of the early phase was more pronounced (55%) than inhibition of the late phase (30%).

In control cells, the capacitance trace appearing after the 1st pulse clearly showed a very short phase of continuing exocytosis preceding a following phase of endocytosis. After the 2nd pulse, only the endocytosis phase existed after the end of the pulse, thus the rates of early endocytosis were determined as the slopes of the capacitance traces for the 300 ms period following the 2nd pulse and normalized by cell size (Fig. 1*C*, -23.8 ± 1.4 fF pF^{-1} s^{-1}, $n = 34$ cells). The late endocytosis occurred at a much lower rate. Fitted with a decaying single exponential, the late endocytosis trace proceeded with a time constant (τ) of 4.0 ± 0.2 s, and the initial rate for the late endocytosis was estimated as the amplitude of retrieved membrane ($\Delta C_m/_{late\text{-}endo}$) divided by τ (Fig. 1*C*, -12.6 ± 1.3 fF pF^{-1} s^{-1}). In the presence of NA, the early endocytosis was not apparent until after the 2nd pulse and showed a slower rate of -13.3 ± 1.1 fF pF^{-1} s^{-1} (Fig. 1*C*, $n = 28$ cells, $P < 0.01$). Although the late phase proceeded with a similar time constant to the control cells ($\tau = 5.2 \pm 0.7$ s, n.s.), the initial rate of the late endocytosis was also lower in NA-treated cells (Fig. 1*C*, -6.9 ± 0.6 fF pF^{-1} s^{-1}, $P < 0.05$) because of the smaller amplitude of ΔC_m /$_{late\text{-}endo}$.

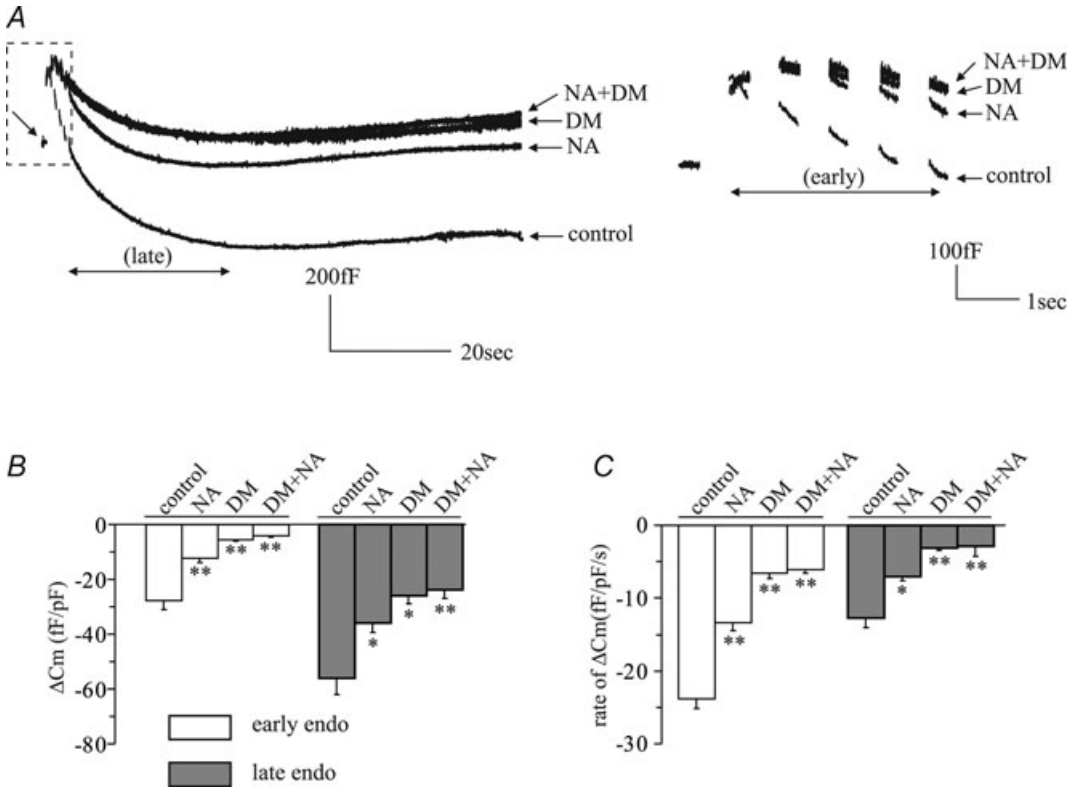

Figure 1. NA and deltamethrin inhibit endocytosis
A, a 500 ms pulse train from −70 mV to +10 mV (with 300 ms interpulse intervals) followed by ∼75 s of recording with the cell membrane clamped at −70 mV was applied in control, NA-, deltamethrin- and deltamethrin+NA-treated cells. The entire recordings are present on the left, and the pulse-stimulating parts of the traces (as marked) are on an expanded time scale on the right. The arrow in the dashed square indicates the cell capacitances before the pulse train. Arrows also indicate the experimental conditions. *B* and *C*, summaries of the effects of NA and deltamethrin on endocytosis (ΔC_m normalized as fF pF^{-1}) and endocytotic rates (ΔC_m normalized as fF pF^{-1} s^{-1}), respectively. These effects were characterized with respect to early and late endocytosis. The traces in the figure were averaged from 16–34 cells. $^*P < 0.05$, $^{**}P < 0.01$, #n.s.

The effect of the calcineurin inhibitor deltamethrin on endocytosis

Calcineurin inhibitors are known to block endocytosis (Enan & Matsumura, 1992; Groblewski *et al.* 1994) by inhibiting a cascade of protein dephosphorylations essential for endocytosis to occur (Cousin & Robinson, 2001). Inhibition of endocytosis by NA was therefore compared with that of a well-known calcineurin antagonist deltamethrin (Enan & Matsumura, 1992). Deltamethrin (final concentration 1 μM) was dialysed into the cell via the whole-cell patch pipette. Before stimulation, ∼5 min was allowed for the compound to reach equilibrium between the pipette solution and the cytosol. Deltamethrin was an effective inhibitor of endocytosis in these cells (Fig. 1) (deltamethrin: $\Delta C_m/_{\text{early-endo}}$, -5.5 ± 0.5 fF pF^{-1}, $P < 0.05$; $\Delta C_m/_{\text{late-endo}}$, -25.9 ± 2.8 fF pF^{-1}, $P < 0.05$, $n = 16$ cells). The combination of NA and deltamethrin was not more effective than deltamethrin alone (deltamethrin+NA: $\Delta C_m/_{\text{early-endo}}$, -4.0 ± 0.6 fF pF^{-1}, n.s.; $\Delta C_m/_{\text{late-endo}}$, -23.8 ± 3.0 fF pF^{-1}, n.s., $n = 17$ cells). Again, inhibition was more pronounced for early endocytosis (80%) than for late endocytosis (50%). Similar to the effect of NA, deltamethrin slowed the rate of early endocytosis significantly (Fig. 1*C*, deltamethrin, -6.5 ± 0.8 fF pF^{-1} s^{-1}, $n = 16$ cells, $P < 0.01$; deltamethrin+NA; -6.1 ± 0.5 fF pF^{-1} s^{-1}, $n = 17$ cells, $P < 0.01$). Compared to the control cells, the time constants of the late endocytosis were increased to 8.4 ± 0.7 s (deltamethrin, $P < 0.01$) and 8.9 ± 0.9 s (deltamethrin+NA, $P < 0.05$), respectively. Deltamethrin effectively inhibited the late endocytosis rate (deltamethrin, -3.1 ± 0.3 fF pF^{-1} s^{-1}, $P < 0.05$).

NA reduces the number of endocytotic events and does not affect vesicle size

To determine whether the inhibition of endocytosis by NA and by deltamethrin was due to a decrease in endocytotic vesicle size or due to a reduction in the number of endocytotic events, cell-attached patch capacitance measurements were performed (Debus & Lindau, 2000). The cells were incubated in the extracellular solution containing NA (5 μM) or deltamethrin (10 μM) for ∼5 min before the pipette was sealed onto a membrane patch and capacitance was recorded for 10 min. Downward capacitance steps indicating single vesicle endocytosis (Fig. 2*A*, Im) were only counted when their amplitude was >0.1 fF because due to variability in noise, smaller steps were not reliably identified. Typically (Fig. 2*A*) the fission pore closure manifests itself as a transient increase in the real part (Re) of the patch admittance on a time scale of 5–200 ms associated with a time-resolved decrease in the imaginary part (Im). From the Im and Re traces, the time courses of fission pore conductance (G_p) and vesicle capacitance (C_v) were calculated. Narrow, low conductance fission pores lead to transient increases in the real part of the patch admittance (Fig. 2*A*, Re) (Dernick *et al.* 2003), which are evident for the larger events (Fig. 2*Aa–c*) but were usually undetectable for small events (Fig. 2*Aa*) due to the low signal-to-noise ratio of these events. The mean step size of vesicles with a detectable change in the Re trace indicating the fission pore properties was ∼1 fF (control, 1.1 ± 0.1 fF, $n = 113$; NA, 0.9 ± 0.1 fF, $n = 77$ events; deltamethrin, 1.0 ± 0.3 fF, $n = 44$ events). The capacitance steps without a detectable change in the Re trace had a mean size of ∼0.25 fF (control, 0.27 ± 0.03 fF, $n = 553$ events; NA, 0.25 ± 0.01 fF, $n = 175$; deltamethrin, 0.25 ± 0.04 fF, $n = 176$ events). The durations of the transients in the Re trace were usually shorter than 100 ms (Fig. 2*Ab*). Transients with long duration that increased gradually until abruptly returning to the baseline (Fig. 2*Ac*) were rare. The total number of events per cell occurring during the 10 min recording was reduced by ∼50% by both NA and deltamethrin. The reduction affected both large and small endocytotic events, differentiated by whether there was a detectable transient in the Re trace, similarly (Fig. 2*B*). Accordingly, the cumulative distributions of endocytotic capacitance step size were also similar in control, NA and deltamethrin-treated conditions (Fig. 2*C*). These data are presented also as gaussian distributions in supplemental Fig. 1. Thus, inhibition of endocytosis by NA and by deltamethrin is due to a decrease in the number of events without a significant change in vesicle size and the effects are similar on endocytotic vesicles of different sizes.

NA selectively inhibits rapid fission pore closure

The dynamics of fission pore closure reflect the molecular events leading to fission. Fission pore dynamics could be quantified for the large endocytic vesicles by measuring the lifetime of each fission pore and final fission pore conductance before abrupt closure (Fig. 2*Ab* and *c*). The final G_p was taken at a time point where the C_v trace decreased 10–20% from the full vesicle capacitance to account for the time resolution of the admittance measurement. The lifetime of the fission pore (duration) was taken as the time between its final closure and the time where G_p decreased to 2 nS, which was always after the slope of G_p had decreased sharply, indicating rapid fission pore closure. The final fission pore conductance before abrupt closure in deltamethrin-treated cells (0.16 ± 0.03 nS) and NA-treated cells (0.17 ± 0.02 nS), tended to be somewhat smaller than in the control cells (0.23 ± 0.03 nS), although the difference was not statistically significant. Therefore, it is uncertain if the final fission pore structure is different in the control

cells and the deltamethrin- and NA-treated cells. For a conservative comparison of fission pore duration, we calculated the median fission pore duration for each patch and then the mean of the median values (Fig. 3*A*). The average fission pore durations determined in this way were not significantly different between the control cells (46.2 ± 9.8 ms) and deltamethrin-treated cells (62.8 ± 33.7 ms, n.s.) but were significantly increased in NA-treated cells (199.7 ± 64.3 ms, $P < 0.05$). Under control conditions, the final fission pore conductance reported here is slightly larger, and the time for fission pore closure is shorter than those reported previously (MacDonald *et al.* 2005). The likely reasons for these differences are that we used a lock-in amplifier with a faster filter setting in order to apply the increased time resolution to the measurement of the rapid fission mode. More importantly, different analysis methods were used in the two reports. MacDonald *et al.* quantified the kinetics of fission pore closure by exponential fits of the fission pore conductance trace, whereas in our case the time course was

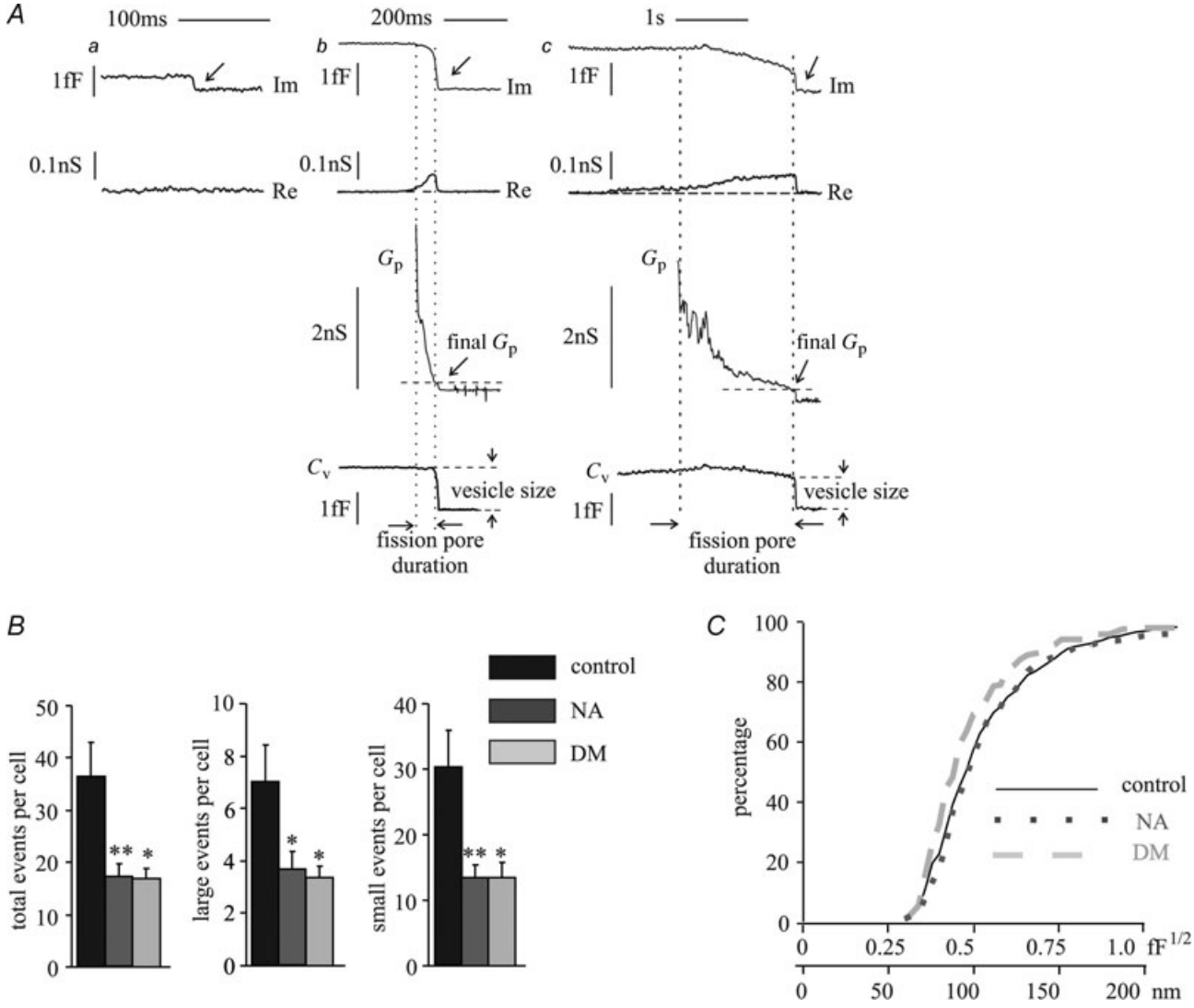

Figure 2. NA reduces the frequency of endocytotic events without changing the vesicle size
Individual endocytotic events were resolved by cell-attached capacitance measurements. *A*, examples of three types of endocytotic events recorded. Re and Im, the real and imaginary parts of the patch admittance change, respectively, with arrows indicating single endocytotic events; G_p, fission pore conductance; C_v, vesicle capacitance indicating the vesicle size. *Aa*, a small endocytotic event without a detectable Re change; *Ab*, a large event with a detectable Re change; *Ac*, a rare large event with a long fission pore duration and a detectable Re change that gradually reached the maximum and abruptly returned back to the baseline. The recording time for each cell was ~10 min. *B*, the total events per cell for all endocytotic events (total, large and small) recorded from control, NA- and deltamethrin-treated cells. *C*, the cumulative distributions of endocytotic vesicle sizes (expressed as the square roots of C_v values, and the corresponding values of the vesicle diameters) under corresponding experimental conditions. Data were analysed from 16–21 cells. $^*P < 0.05$, $^{**}P < 0.01$, #n.s.

quantified as the fission pore duration. In our recordings an exponential fit appeared inappropriate for many events. The different methods of analysis also affect somewhat the determination of the final fission pore conductance.

To characterize the fission dynamics in more detail, fission pore survival curves were constructed based on all the measured fission pore lifetimes from all patches (Fig. 3*B*). The survival curves (continuous lines) were not well fitted by a single exponential (dotted lines, with r^2 values of 0.92, 0.91 and 0.96 for the control, NA and deltamethrin-treated cells, respectively) but could be fitted well assuming a double exponential decay (dashed lines, with r^2 values of 0.99, 0.98 and 0.99 for the control, NA and deltamethrin-treated cells, respectively) indicating two distinct endocytotic fission mechanisms with different kinetics. These define the rapid and slow components. For control- and deltamethrin-treated cells the rapid mechanisms were dominant with ∼84% of the amplitudes, and exhibited similar time constants (control, $\tau_{rapid} = 37.6 \pm 0.3$ ms, $\tau_{slow} = 352 \pm 4.8$ ms; deltamethrin, $\tau_{rapid} = 24.9 \pm 0.4$ ms, $\tau_{slow} = 269 \pm 5.5$ ms). For NA-treated cells the contribution of the rapid component was reduced from 84% to 45% with similar time constants for the two kinetic components ($\tau_{rapid} = 42.4 \pm 1.1$ ms, $\tau_{slow} = 424 \pm 2.4$ ms). NA thus selectively inhibited the rapid fission events by 73% from an average of 5.9 ± 1.2 events patch^{-1} in control cells to 1.6 ± 0.3 events patch^{-1} in NA-treated cells. This decrease is only partly compensated by an increased occurrence of slow fission pore closures from 1.1 ± 0.2 (control) to 2.1 ± 0.4 (NA) events patch^{-1}. In contrast, both the frequencies of rapid and slow events were proportionally inhibited by deltamethrin (rapid, 2.3 ± 0.4 events cell^{-1}; slow, 0.5 ± 0.1 events cell^{-1}), the fusion pore lifetime kinetics were unchanged (Fig. 3*B*). These results show that inhibition of endocytosis by NA and deltamethrin involve distinct molecular mechanisms. NA specifically inhibits the rapid mode of fission and thus presumably a late step in endocytosis.

Receptor and G protein involvement in the hormonal control of endocytosis

NA inhibits insulin secretion via the coupling of α_2-adrenergic receptors and the subsequent activation of G_i/G_o proteins (Komatsu *et al.* 1995; Sharp, 1996). To determine whether inhibition of endocytosis by NA is also due to binding to α_2-adrenergic receptors, yohimbine, a classical α_2-adrenergic receptor antagonist (Niddam *et al.* 1990), was added to the extracellular solution. Two groups of cells were separately treated with 10 μM yohimbine alone or with the combination of yohimbine and NA (Fig. 4*A* and Supplemental Fig. 2*A* in Supplemental material, available online only). In the presence of yohimbine, NA-induced inhibition of early and late endocytosis was abolished ($\Delta C_m/_{early\text{-}endo}$: yohimbine, -31.4 ± 4.4 fF pF^{-1}, $n = 21$ cells; yohimbine+NA,

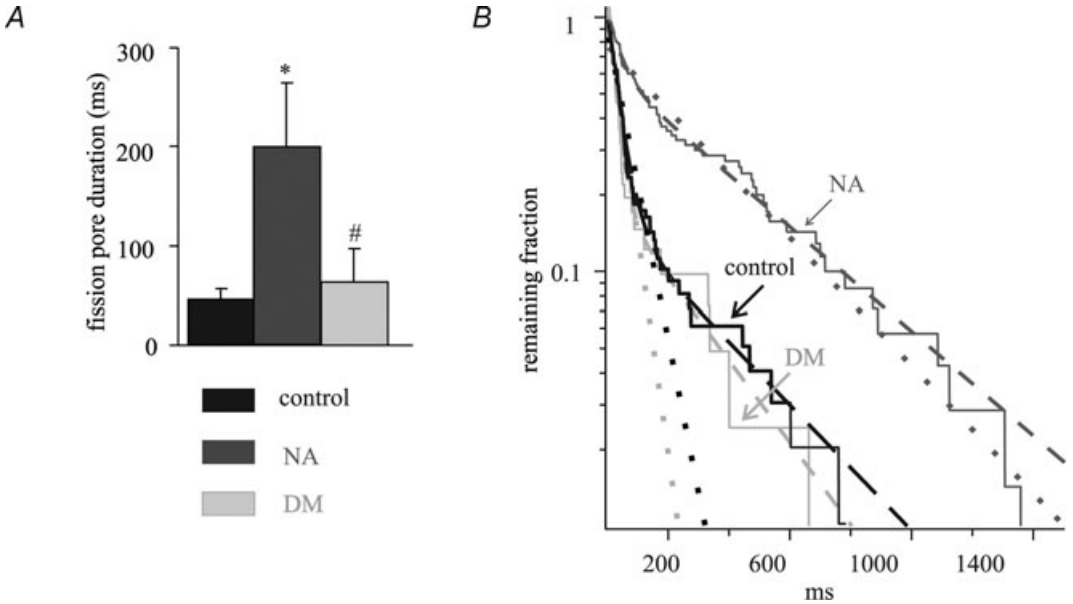

Figure 3. NA preferentially inhibits the rapid fission pore closure
A, the mean of the median values of fission pore duration for each patch under control and experimental conditions. *B*, the survival curves (continuous lines) of fission pore duration for control and test cells were plotted on a logarithmic scale. The survival curves are fitted with single exponential decays (dotted lines) and double exponential decays (dashed lines). The arrows indicate the different experimental conditions. Data were analysed from all the events obtained in Fig. 2. $^*P < 0.05$, $^{**}P < 0.01$, #n.s.

-27.2 ± 3.8 fF pF^{-1}, $n = 20$ cells, n.s. $\Delta C_m/_{\text{late-endo}}$: yohimbine, -58.7 ± 5.3 fF pF^{-1}; yohimbine+NA, -54.4 ± 5.6, n.s.). NA inhibition of endocytosis is therefore mediated by α_2-adrenergic receptors, as expected. Unexpectedly, however, PTX-pretreatment of the cells (150 ng ml^{-1}, >24 h) failed to block the inhibition of endocytosis by NA (Fig. 4*A* and Supplemental Fig. 2*A*, $\Delta C_m/_{\text{early-endo}}$: PTX, -29.9 ± 4.2 fF pF^{-1}, $n = 20$ cells; PTX+NA, -11.8 ± 2.1 fF pF^{-1}, $n = 20$ cells, $P < 0.01$. $\Delta C_m/_{\text{late-endo}}$: PTX, -60.1 ± 6.0 fF pF^{-1}; PTX+NA, -42.2 ± 3.3, $P < 0.05$) indicating that the inhibition was not mediated by the PTX-sensitive G_i/G_o proteins. The rates of early- and late-endocytosis determined under test conditions mentioned above are present in Fig. 4*B* and in Supplemental Table 1 (see online Supplemental material). To test the possibility that hormonal inhibition of endocytosis is mediated by G_z, the only PTX-insensitive member of the G_i/G_o family of

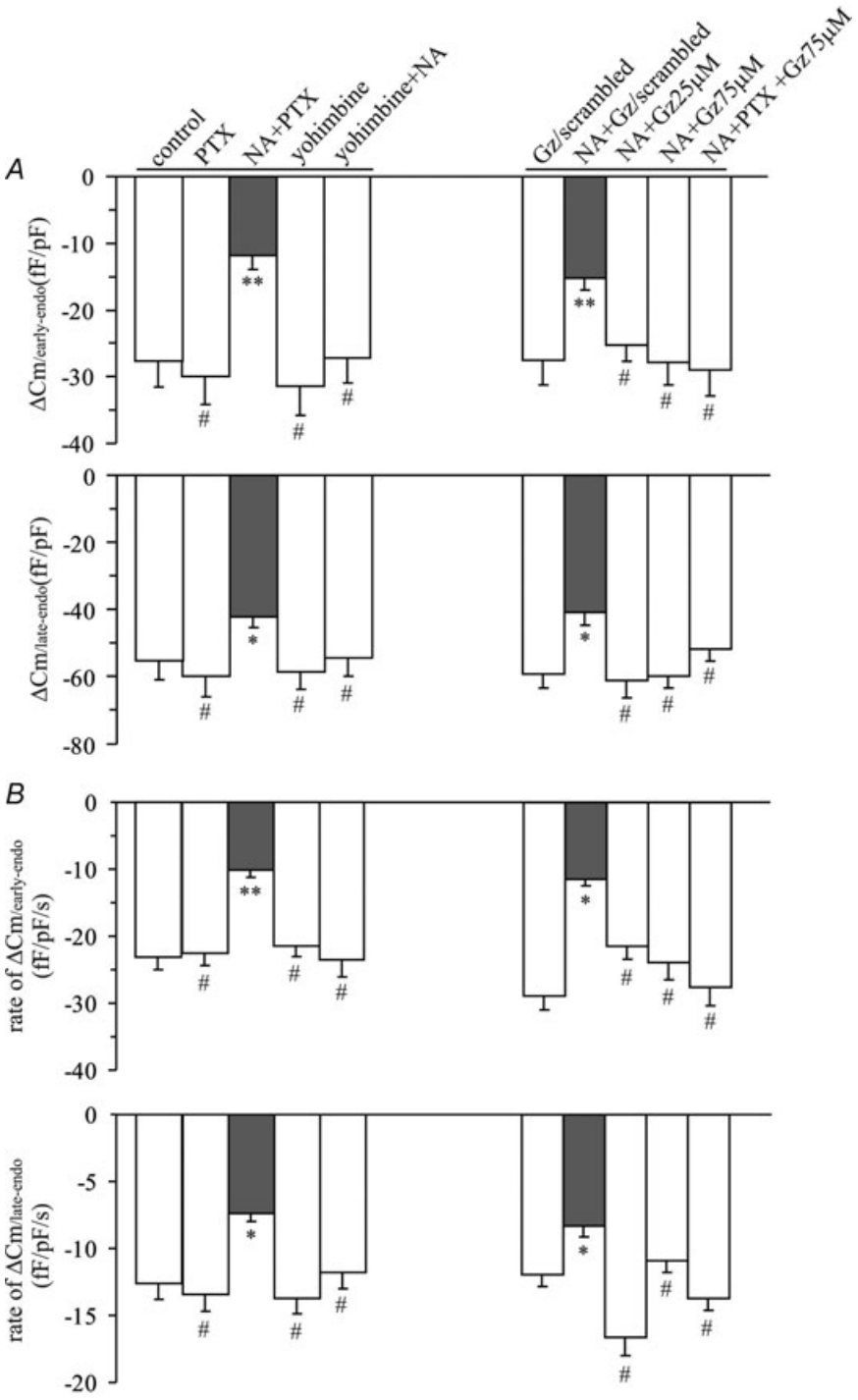

Figure 4. NA inhibits endocytosis via the α_2-adrenergic receptor, and the heterotrimeric G protein G_z is involved in the inhibitory effects of NA
The signalling pathways in the hormonally mediated inhibition of endocytosis were investigated in the presence of PTX, yohimbine and two different concentrations of a G_z-blocking peptide. *A*, summaries of the endocytotic actions studied in various test conditions (as labelled), in the early (upper panel) and late (lower panel) phases. *B*, summaries of endocytotic rates under the same experimental conditions as labelled in *A*. Data were analysed from 19–25 cells for each experimental condition. Protocols were analogous to those used in the experiments of Fig. 1 and Supplemental Fig. 1. No specific effects of the G_z-blocking peptide alone on exocytosis were observed under these experimental conditions (data not shown). $^*P < 0.05$, $^{**}P < 0.01$, #n.s.

G proteins, a synthetic peptide mimicking the C-terminal 11 amino acids of the $G\alpha_z$ subunit was dialysed into the cell via the patch pipette at two different concentrations. Such peptides are known to block the interaction of G proteins with their activated receptors and thus eliminate their effects in cells (Gilchrist *et al.* 1998, 2001, 2002) including the INS 832/13 cell (Zhao *et al.* 2008). Before stimulation, ∼5 min were allowed for the peptide to reach equilibrium between the pipette solution and the cytosol. As shown, the G_z-blocking peptide, at concentrations of 25 and 75 μM, significantly reduced NA inhibition of endocytosis (Fig. 4*A*, Supplemental Fig. 2*B* and Supplemental Table 2). Further, the experiments were repeated with cells pretreated with PTX (150 ng ml^{-1}, >24 h). As shown in Supplemental Fig. 2*B* and Table 1, inhibition of endocytosis was not influenced by PTX, which is consistent with NA inhibition of endocytosis via G_z. To exclude possible non-specific peptide effects, control experiments were performed using a scrambled peptide with the same 11 amino acids in random order ($G_z/_{scrambled}$, 75 μM, Supplemental Fig. 1*B*). This peptide had no effect on the inhibition of endocytosis by NA (Fig. 4*B* and Supplemental Table 2). The rates of early and late endocytosis in the absence and presence of the G_z blocking peptide and the scrambled peptide were determined and are shown in Fig. 4*B* and in Supplemental Table 1. These data imply that the hormonal regulation of endocytosis is mediated by G_z.

Discussion

Endocytosis in the β-cell was first documented in 1973 when increased uptake of horseradish peroxidase was seen following glucose-stimulated insulin release (Orci *et al.* 1973). The authors rightly surmised that exocytosis–endocytosis coupling was essential for membrane recycling following increased secretory activity. Following a hiatus of 13 years, subsequent studies occurred sporadically (Orci *et al.* 1986; Carpentier *et al.* 1989; Ammala *et al.* 1993; Proks & Ashcroft, 1995; Eliasson *et al.* 1996) until more recently (Nagamatsu *et al.* 2001; Hoy *et al.* 2002; Ohara-Imaizumi *et al.* 2002; Kuliawat *et al.* 2004; Ma *et al.* 2004; Tsuboi *et al.* 2004; MacDonald *et al.* 2005; Hanna *et al.* 2008; Kimura *et al.* 2008). The nature of the exocytotic events and the extent of full fusion and 'kiss and run' are important to the understanding of endocytosis in the β-cell (Ma *et al.* 2004; Tsuboi *et al.* 2004; MacDonald & Rorsman, 2007; Hanna *et al.* 2008) which involve different modes of endocytosis. Our experiments show that both compensatory and excess endocytosis occur in INS 832/13 cells. Excess endocytosis was previously described in chromaffin cells following a high level of Ca^{2+} influx (Thomas *et al.* 1994; Smith & Neher, 1997). The excess endocytotic activity is resistant to 'wash-out' persisting in the whole-cell patch-clamp configuration without significant decay over a recording time exceeding 5 min (Smith & Neher, 1997). Because of the occurrence of excess membrane retrieval, our averaged traces show that the plasma membrane capacitance decreased to a value below the pre-stimulus baseline and remained there for the duration of the recordings. In chromaffin cells, excess endocytosis occurs in response to Ca^{2+} entry associated with an integrated Ca^{2+} current of ∼70–90 pC or higher (Smith & Neher, 1997; Engisch & Nowycky, 1998). The estimated Ca^{2+} influx during the single depolarizing pulse of 500 ms in our study is close to 150 pC. This value is well above the threshold that causes excess endocytosis in chromaffin cells.

Such a high Ca^{2+} influx abolished the hormonal inhibition of exocytosis, which is consistent with two previously reported observations, (1) that serotonin-induced inhibition of neurotransmitter release (Blackmer *et al.* 2001) is mediated by the $\beta\gamma$ subunit of a specific heterotrimeric G protein that blocks the binding of synaptotagmin to SNAP-25 and thereby prevents exocytosis, and (2) that increased Ca^{2+} influx overcomes the serotonin-induced inhibition of exocytosis by an enhancement of the Ca^{2+}-dependent synaptotagmin binding to SNAP-25, thus displacing $\beta\gamma$ and allowing exocytosis to proceed (Blackmer *et al.* 2005; Gerachshenko *et al.* 2005; Photowala *et al.* 2006) and by our recent report that the inhibition of exocytosis in the β-cell by NA was abolished by increased Ca^{2+} influx (Zhao *et al.* 2010, accompanying paper). It was this finding that enabled the detection of the inhibition of endocytosis by NA.

NA inhibits endocytosis by a mechanism distinct from calcineurin inhibitors

We have shown here that NA is a powerful inhibitor of endocytosis. Deltamethrin inhibits endocytosis because it is a calcineurin inhibitor and therefore blocks the initiating step in the dephosphorylation of a group of proteins implicated in endocytosis. These proteins include amphiphysin, synaptojanin, AP180, epsin, dynamins, clathrin and clathrin adaptors, some of which have been identified in insulin-secreting cells (Cousin & Robinson, 2001; MacDonald & Rorsman, 2007). As a result of their action to inhibit the first step in the mechanism of endocytosis, the calcineurin inhibitors have only the simple action of preventing endocytosis from occurring and have no effect on vesicle size, fission kinetics or other aspects of the mechanisms involved. Similarly, NA inhibits endocytosis by reducing the frequency of endocytotic events without changing the endocytosed vesicle size, although it does affect the fission pore kinetics. In these insulin-secreting cells endocytosis occurs in two kinetically distinct phases reminiscent of those previously reported for chromaffin cells (Smith & Neher,

1997). NA inhibited both the early and the late phases of endocytosis, although inhibition of the early phase was more pronounced. As expected, deltamethrin significantly increased the time constant of slow endocytosis about twofold. In contrast, NA reduced the amplitude and initial rate of slow endocytosis in parallel with no change in the time constant of the slow phase, indicating that NA inhibits endocytosis by a mechanism that is distinct from that of the calcineurin inhibitor deltamethrin. Further evidence that NA and deltamethrin have different modes of action is the selective inhibition of the rapid fission pore closure by NA.

Interestingly, the NA-induced inhibition of endocytosis is PTX-insensitive which contrasts with the PTX-sensitivity of its inhibitory effects on exocytosis. Also, the inhibition of endocytosis is attenuated by a G_z-blocking peptide, a finding that indicates the involvement of the heterotrimeric G_z protein in the hormonal regulation of endocytosis. While G_z has not previously been linked to NA, it is present in these β-cells and is known to be activated by PGE_1 (Kimple *et al.* 2005, 2008).

Inhibition of endocytosis by NA is a novel finding that has obvious physiological significance. Under normal conditions, when the β-cell is stimulated, increased exocytosis due to elevated $[Ca^{2+}]_i$ is followed promptly by $[Ca^{2+}]_i$-stimulated endocytosis. Thus, the addition and removal of vesicle membrane to and from the plasma membrane is balanced and cell volume remains constant. However, under conditions in which $[Ca^{2+}]_i$ is elevated yet insulin secretion is inhibited, e.g. an arginine-stimulated cell in which secretion is blocked by NA, stimulation of endocytosis by the raised $[Ca^{2+}]_i$ must also be inhibited to prevent a reduction in cell volume.

NA selectively inhibits a specific fission mechanism

The fission event proceeds by a gradual narrowing and/or lengthening of the neck connecting the endocytotic vesicle to the extracellular space as indicated by a gradual decrease in fission pore conductance. However, the ultimate pinching off involves an abrupt stepwise change in fission pore conductance from an average value of ~210 pS, which is remarkably similar to the fission event in chromaffin cells (Dernick *et al.* 2003). The gradual reduction in fission pore conductance preceding this final step proceeds with two different kinetic components associated with fission pore lifetimes of τ_{rapid} ~30 ms and of τ_{slow} ~350 ms. NA preferentially targets the rapid fission events, while deltamethrin inhibits the fast and slow fission pore closures equally. This was to be expected of deltamethrin because it inhibits calcineurin, the first enzyme that is activated in the cascade of events from increased $[Ca^{2+}]_i$ to endocytosis and is thus unlikely to have any effect on downstream events associated with the mechanisms of endocytosis. Presumably, membrane targeted for endocytosis is internalized by both fission mechanisms. The selective inhibition of the rapid fission pore closure by NA provides further strong evidence that its specific mechanism of action is different from that of deltamethrin. As it appears that the target of NA is a late step involved in rapidly pinching off the endocytotic vesicle, future studies must be directed towards finding the site of interaction of G_z with one or more of the proteins involved in fission pore formation and closure.

In summary, NA specifically inhibits endocytosis and selectively affects the rapid fission machinery, an action that is mechanistically different from the action of the calcineurin antagonist deltamethrin. The observed hormonal inhibition of endocytosis, a previously unknown action of NA, is mediated by activation of G_z. These results reveal hormonal control of endocytosis as a novel mechanism in insulin-secreting cells but one that is also likely to occur in many other cell types.

References

Ales E, Tabares L, Poyato JM, Valero V, Lindau M & Alvarez de Toledo G (1999). High calcium concentrations shift the mode of exocytosis to the kiss-and-run mechanism. *Nat Cell Biol* **1**, 40–44.

Ammala C, Eliasson L, Bokvist K, Larsson O, Ashcroft FM & Rorsman P (1993). Exocytosis elicited by action potentials and voltage-clamp calcium currents in individual mouse pancreatic B-cells. *J Physiol* **472**, 665–688.

Artalejo CR, Elhamdani A & Palfrey HC (2002). Sustained stimulation shifts the mechanism of endocytosis from dynamin-1-dependent rapid endocytosis to clathrin- and dynamin-2-mediated slow endocytosis in chromaffin cells. *Proc Natl Acad Sci U S A* **99**, 6358–6363.

Blackmer T, Larsen EC, Bartleson C, Kowalchyk JA, Yoon EJ, Preininger AM, Alford S, Hamm HE & Martin TF (2005). G protein $\beta\gamma$ directly regulates SNARE protein fusion machinery for secretory granule exocytosis. *Nat Neurosci* **8**, 421–425.

Blackmer T, Larsen EC, Takahashi M, Martin TF, Alford S & Hamm HE (2001). G protein $\beta\gamma$ subunit-mediated presynaptic inhibition: regulation of exocytotic fusion downstream of Ca^{2+} entry. *Science* **292**, 293–297.

Carpentier JL, Sawano F, Geiger D, Gorden P, Perrelet A & Orci L (1989). Potassium depletion and hypertonic medium reduce "non-coated" and clathrin-coated pit formation, as well as endocytosis through these two gates. *J Cell Physiol* **138**, 519–526.

Cousin MA & Robinson PJ (2001). The dephosphins: dephosphorylation by calcineurin triggers synaptic vesicle endocytosis. *Trends Neurosci* **24**, 659–665.

Debus K & Lindau M (2000). Resolution of patch capacitance recordings and of fusion pore conductances in small vesicles. *Biophys J* **78**, 2983–2997.

Dernick G, Alvarez de Toledo G & Lindau M (2003). Exocytosis of single chromaffin granules in cell-free inside-out membrane patches. *Nat Cell Biol* **5**, 358–362.

Eliasson L, Proks P, Ammala C, Ashcroft FM, Bokvist K, Renstrom E, Rorsman P & Smith PA (1996). Endocytosis of secretory granules in mouse pancreatic β-cells evoked by transient elevation of cytosolic calcium. *J Physiol* **493**, 755–767.

Enan E & Matsumura F (1992). Specific inhibition of calcineurin by type II synthetic pyrethroid insecticides. *Biochem Pharmacol* **43**, 1777–1784.

Engisch KL & Nowycky MC (1998). Compensatory and excess retrieval: two types of endocytosis following single step depolarizations in bovine adrenal chromaffin cells. *J Physiol* **506**, 591–608.

Gerachshenko T, Blackmer T, Yoon EJ, Bartleson C, Hamm HE & Alford S (2005). G$\beta\gamma$ acts at the C terminus of SNAP-25 to mediate presynaptic inhibition. *Nat Neurosci* **8**, 597–605.

Gilchrist A, Li A & Hamm HE (2002). Gα COOH-terminal minigene vectors dissect heterotrimeric G protein signaling. *Sci STKE* **2002**, PL1.

Gilchrist A, Mazzoni MR, Dineen B, Dice A, Linden J, Proctor WR, Lupica CR, Dunwiddie TV & Hamm HE (1998). Antagonists of the receptor-G protein interface block G_i-coupled signal transduction. *J Biol Chem* **273**, 14912–14919.

Gilchrist A, Vanhauwe JF, Li A, Thomas TO, Voyno-Yasenetskaya T & Hamm HE (2001). Gα minigenes expressing C-terminal peptides serve as specific inhibitors of thrombin-mediated endothelial activation. *J Biol Chem* **276**, 25672–25679.

Groblewski GE, Wagner AC & Williams JA (1994). Cyclosporin A inhibits Ca^{2+}/calmodulin-dependent protein phosphatase and secretion in pancreatic acinar cells. *J Biol Chem* **269**, 15111–15117.

Hanna ST, Pigeau GM, Galvanovskis J, Clark A, Rorsman P & Macdonald PE (2008). Kiss-and-run exocytosis and fusion pores of secretory vesicles in human β-cells. *Pflugers Arch* **457**, 1343–1350.

Harata NC, Aravanis AM & Tsien RW (2006). Kiss-and-run and full-collapse fusion as modes of exo-endocytosis in neurosecretion. *J Neurochem* **97**, 1546–1570.

Hoy M, Efanov AM, Bertorello AM, Zaitsev SV, Olsen HL, Bokvist K, Leibiger B, Leibiger IB, Zwiller J, Berggren PO & Gromada J (2002). Inositol hexakisphosphate promotes dynamin I-mediated endocytosis. *Proc Natl Acad Sci U S A* **99**, 6773–6777.

Jahn R, Lang T & Sudhof TC (2003). Membrane fusion. *Cell* **112**, 519–533.

Jarousse N & Kelly RB (2001). Endocytotic mechanisms in synapses. *Curr Opin Cell Biol* **13**, 461–469.

Kimple ME, Joseph JW, Bailey CL, Fueger PT, Hendry IA, Newgard CB & Casey PJ (2008). Gα_z negatively regulates insulin secretion and glucose clearance. *J Biol Chem* **283**, 4560–4567.

Kimple ME, Nixon AB, Kelly P, Bailey CL, Young KH, Fields TA & Casey PJ (2005). A role for G_z in pancreatic islet β-cell biology. *J Biol Chem* **280**, 31708–31713.

Kimura T, Kaneko Y, Yamada S, Ishihara H, Senda T, Iwamatsu A & Niki I (2008). The GDP-dependent Rab27a effector coronin 3 controls endocytosis of secretory membrane in insulin-secreting cell lines. *J Cell Sci* **121**, 3092–3098.

Komatsu M, McDermott AM, Gillison SL & Sharp GW (1995). Time course of action of pertussis toxin to block the inhibition of stimulated insulin release by norepinephrine. *Endocrinology* **136**, 1857–1863.

Kuliawat R, Kalinina E, Bock J, Fricker L, McGraw TE, Kim SR, Zhong J, Scheller R & Arvan P (2004). Syntaxin-6 SNARE involvement in secretory and endocytic pathways of cultured pancreatic β-cells. *Mol Biol Cell* **15**, 1690–1701.

Lindau M & Neher E (1988). Patch-clamp techniques for time-resolved capacitance measurements in single cells. *Pflugers Arch* **411**, 137–146.

Ma L, Bindokas VP, Kuznetsov A, Rhodes C, Hays L, Edwardson JM, Ueda K, Steiner DF & Philipson LH (2004). Direct imaging shows that insulin granule exocytosis occurs by complete vesicle fusion. *Proc Natl Acad Sci U S A* **101**, 9266–9271.

MacDonald PE, Eliasson L & Rorsman P (2005). Calcium increases endocytotic vesicle size and accelerates membrane fission in insulin-secreting INS-1 cells. *J Cell Sci* **118**, 5911–5920.

MacDonald PE & Rorsman P (2007). The ins and outs of secretion from pancreatic β-cells: control of single-vesicle exo- and endocytosis. *Physiology (Bethesda)* **22**, 113–121.

Murthy VN & De Camilli P (2003). Cell biology of the presynaptic terminal. *Annu Rev Neurosci* **26**, 701–728.

Nagamatsu S, Nakamichi Y, Watanabe T, Matsushima S, Yamaguchi S, Ni J, Itagaki E & Ishida H (2001). Localization of cellubrevin-related peptide, endobrevin, in the early endosome in pancreatic β-cells and its physiological function in exo-endocytosis of secretory granules. *J Cell Sci* **114**, 219–227.

Niddam R, Angel I, Bidet S & Langer SZ (1990). Pharmacological characterization of alpha-2 adrenergic receptor subtype involved in the release of insulin from isolated rat pancreatic islets. *J Pharmacol Exp Ther* **254**, 883–887.

Ohara-Imaizumi M, Nakamichi Y, Tanaka T, Katsuta H, Ishida H & Nagamatsu S (2002). Monitoring of exocytosis and endocytosis of insulin secretory granules in the pancreatic β-cell line MIN6 using pH-sensitive green fluorescent protein (pHluorin) and confocal laser microscopy. *Biochem J* **363**, 73–80.

Orci L, Malaisse-Lagae F, Ravazzola M, Amherdt M & Renold AE (1973). Exocytosis-endocytosis coupling in the pancreatic β-cell. *Science* **181**, 561–562.

Orci L, Ravazzola M, Amherdt M, Brown D & Perrelet A (1986). Transport of horseradish peroxidase from the cell surface to the Golgi in insulin-secreting cells: preferential labelling of cisternae located in an intermediate position in the stack. *EMBO J* **5**, 2097–2101.

Photowala H, Blackmer T, Schwartz E, Hamm HE & Alford S (2006). G protein $\beta\gamma$-subunits activated by serotonin mediate presynaptic inhibition by regulating vesicle fusion properties. *Proc Natl Acad Sci U S A* **103**, 4281–4286.

Proks P & Ashcroft FM (1995). Effects of divalent cations on exocytosis and endocytosis from single mouse pancreatic β-cells. *J Physiol* **487**, 465–477.

Rizzoli SO & Jahn R (2007). Kiss-and-run, collapse and 'readily retrievable' vesicles. *Traffic* **8**, 1137–1144.

Rorsman P, Bokvist K, Ammala C, Arkhammar P, Berggren PO, Larsson O & Wahlander K (1991). Activation by adrenaline of a low-conductance G protein-dependent K^+ channel in mouse pancreatic B cells. *Nature* **349**, 77–79.

Schermerhorn T & Sharp GW (2000). Norepinephrine acts on the K_{ATP} channel and produces different effects on $[Ca^{2+}]_i$ in oscillating and non-oscillating HIT-T15 cells. *Cell Calcium* **27**, 163–173.

Sharp GW (1996). Mechanisms of inhibition of insulin release. *Am J Physiol Cell Physiol* **271**, C1781–C1799.

Sharp GW, Le Marchand-Brustel Y, Yada T, Russo LL, Bliss CR, Cormont M, Monge L & Van Obberghen E (1989). Galanin can inhibit insulin release by a mechanism other than membrane hyperpolarization or inhibition of adenylate cyclase. *J Biol Chem* **264**, 7302–7309.

Sieg A, Su J, Munoz A, Buchenau M, Nakazaki M, Aguilar-Bryan L, Bryan J & Ullrich S (2004). Epinephrine-induced hyperpolarization of islet cells without K_{ATP} channels. *Am J Physiol Endocrinol Metab* **286**, E463–E471.

Smith C & Neher E (1997). Multiple forms of endocytosis in bovine adrenal chromaffin cells. *J Cell Biol* **139**, 885–894.

Thomas P, Lee AK, Wong JG & Almers W (1994). A triggered mechanism retrieves membrane in seconds after Ca^{2+}-stimulated exocytosis in single pituitary cells. *J Cell Biol* **124**, 667–675.

Tsuboi T, McMahon HT & Rutter GA (2004). Mechanisms of dense core vesicle recapture following "kiss and run" ("cavicapture") exocytosis in insulin-secreting cells. *J Biol Chem* **279**, 47115–47124.

Ullrich S & Wollheim CB (1989). Galanin inhibits insulin secretion by direct interference with exocytosis. *FEBS Lett* **247**, 401–404.

Zhao Y, Fang Q, Straub SG, Lindau M & Sharp GWG (2010). Noradrenaline inhibits exocytosis via the G protein $\beta\gamma$ subunit and refilling of the readily releasable granule pool via the $\alpha_{i1/2}$ subunit. *J Physiol* **588**, 3485–3498.

Zhao Y, Fang Q, Straub SG & Sharp GW (2008). Both G_i and G_o heterotrimeric G proteins are required to exert the full effect of norepinephrine on the β-cell K_{ATP} channel. *J Biol Chem* **283**, 5306–5316.

Author contributions

Y.Z. and Q.F. contributed equally to this work. All authors contributed to the conception and design of the experiments and to the writing of the manuscript. They have all approved the final version for publication. The work was performed in the Department of Molecular Medicine and the School of Applied and Engineering Physics, Cornell University, Ithaca, NY 14853, USA.

Acknowledgements

This work was supported by NIH grants R01-54243 (to G.W.G.S.), R01-NS38200 (to M.L.) and a Career Development Award from the Juvenile Diabetes Foundation International (to S.G.S.).